

# Detecting AI-Generated Images via Distributional Deviations from Real Images

Yakun Niu, Yingjian Chen, Lei Zhang\*

Henan Key Laboratory of Big Data Analysis and Processing,

School of Computer and Information Engineering, Henan University

yingjianchen@henu.edu.cn, zhanglei@henu.edu.cn, ykniu@henu.edu.cn

## Abstract

The rapid advancement of generative models has significantly enhanced the quality of AI-generated images, raising concerns about misinformation and the erosion of public trust. Detecting AI-generated images has thus become a critical challenge, particularly in terms of generalizing to unseen generative models. Existing methods using frozen pre-trained CLIP models show promise in generalization but treat the image encoder as a basic feature extractor, failing to fully exploit its potential. In this paper, we perform an in-depth analysis of the frozen CLIP image encoder (CLIP-ViT), revealing that it effectively clusters real images in a high-level, abstract feature space. However, it does not truly possess the ability to distinguish between real and AI-generated images. Based on this analysis, we propose a **Masking-based Pre-trained model Fine-Tuning (MPFT)** strategy, which introduces a **Texture-Aware Masking (TAM)** mechanism to mask textured areas containing generative model-specific patterns during fine-tuning. This approach compels CLIP-ViT to attend to the “distributional deviations” from authentic images for AI-generated image detection, thereby achieving enhanced generalization performance. Extensive experiments on the GenImage and UniversalFakeDetect datasets demonstrate that our method, fine-tuned with only a minimal number of images, significantly outperforms existing approaches, achieving up to 98.2% and 94.6% average accuracy on the two datasets, respectively.

## 1. Introduction

In recent years, the rapid advancement of generative models [10, 26] has significantly improved image generation quality, making it easier to create highly realistic and high-quality images. For example, online platforms such as Mid-Journey [1] allow users to generate convincingly realistic and deceptive images easily. The potential misuse of these

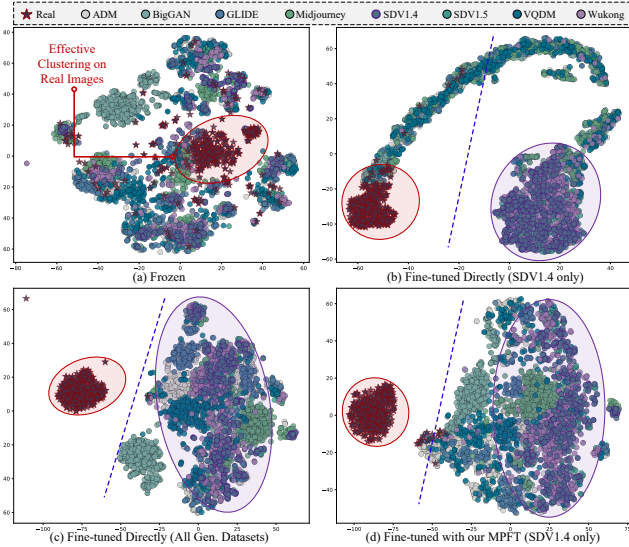


Figure 1. t-SNE [31] visualization of features extracted by pre-trained CLIP-ViT from images generated by eight models in the GenImage dataset. (a) Frozen CLIP-ViT. (b) CLIP-ViT fine-tuned with only SDV1.4-generated images. (c) CLIP-ViT fine-tuned with images generated by **all involved generative models**. (d) CLIP-ViT fine-tuned with our proposed MPFT using **only SDV1.4-generated images**.

models raises serious concerns about the spread of misinformation. Consequently, detecting AI-generated images has become a critical challenge in preserving trust in digital content.

Many existing methods [7, 11–13, 21] achieve promising results in detecting images from seen generative models. However, they often struggle to generalize effectively to unseen generative models. To address this limitation, frozen pre-trained CLIP image encoder (CLIP-ViT) [25] has been widely used for AI-generated image detection [14, 16, 18, 23, 30], demonstrating improved generalization. Nevertheless, these approaches typically treat the frozen CLIP-ViT as a simple feature extractor, lacking in-depth analysis and failing to fully exploit its potential. In this work, we conduct

\*Corresponding author

a visualization-based analysis of the pre-trained CLIP-ViT in the context of AI-generated image detection, uncovering key insights into its feature space that remain unexplored.

## Feature Space Analysis of the Frozen Pre-trained CLIP Image Encoder

For an in-depth exploration of the features extracted by the frozen pre-trained CLIP-ViT [25] for classification, we perform a feature space visualization using the GenImage [39] dataset. The results show that the frozen CLIP-ViT effectively clusters real images (Figure 1, a) in a high-level feature space, benefiting from its strong representation capacity for real images acquired during pre-training on a large-scale dataset of 400 million real images. In this context, most AI-generated images appear as outliers, deviating from the feature distribution of real images. This enables the model to achieve generalized detection across diverse generative models by capturing a universal “distribution shift”—that is, the deviation of generated image features from the compact cluster formed by real images in the high-dimensional feature space—rather than relying on specific low-level forgery artifacts [4, 18, 28, 34]. However, since the pre-trained encoder is not specifically optimized for this task, as reflected by the scattered distribution of AI-generated images, it lacks the ability to directly identify generated content and instead relies solely on the distribution gap for discrimination, which limits its detection accuracy in the absence of task-specific fine-tuning. This naturally raises a straightforward question: Why not fine-tune the CLIP-ViT directly to better adapt to the AI-generated image detection task?

## Limitations of Fine-tuning the Pre-trained CLIP Image Encoder for AI-Generated Image Detection

To answer this, we analyze the impact of fine-tuning on the pre-trained CLIP image encoder using the same GenImage dataset as in the previous analysis. Specifically, we visualize the feature space of CLIP-ViT fine-tuned on a single generative model (SDV1.4) and on a combination of eight generative models. After being fine-tuned on SDV1.4, the model shows clear clustering and separation between real images and SDV1.4-generated images (Figure 1, b). However, it exhibits overfitting, unable to distinguish images generated by other unseen models. This overfitting arises because the fine-tuning process encourages the model to rely on the differences between SDV1.4-generated images and real images for classification, while such unique differences [5, 23] do not exist in images generated by other models, thus limiting its generalization ability. In contrast, when fine-tuned on images generated by all eight models, CLIP-ViT effectively clusters real images and distinguishes them from those generated by all seen models.

Additionally, to further investigate the fine-tuning pro-

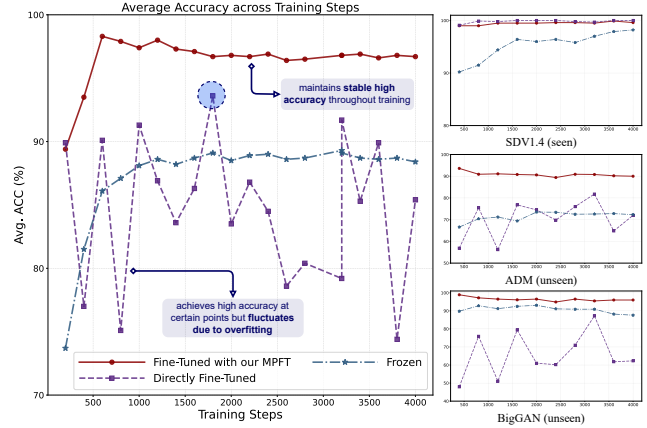


Figure 2. Left: Generalization performance (average accuracy across all 8 subsets of the GenImage test set) of three models: frozen CLIP-ViT with a trainable linear classifier, directly fine-tuned CLIP-ViT, and CLIP-ViT fine-tuned using our MPFT strategy. All models are trained on the SDV1.4 subset of the GenImage training set. Right: Accuracy of the models on the SDV1.4 (seen), ADM (unseen), and BigGAN (unseen) subsets of the GenImage test set.

cess, we analyze the generalization performance of the model during fine-tuning on SDV1.4, as shown in Figure 2. The results demonstrate that while the directly fine-tuned pre-trained CLIP-ViT achieves relatively good performance at certain stages, its generalization ability fluctuates and gradually degrades as fine-tuning progresses (purple line). In contrast, the frozen CLIP-ViT with a trainable linear classifier [23] maintains stable performance throughout (blue line). Similarly, the directly fine-tuned model shows steadily increasing accuracy on the SDV1.4 (seen), but exhibits fluctuating and limited performance on the ADM and BigGAN (both unseen). These observations confirm that: (1) The feature space of the pre-trained CLIP-ViT is compromised due to overfitting to the training data as fine-tuning progresses, causing fluctuations and performance degradation; and (2) The optimal generalization performance is typically reached in the early stage of fine-tuning (within 1,000 steps), suggesting that fine-tuning with the pre-trained CLIP-ViT requires only a small amount of data to achieve peak performance.

## Motivation

Based on the above analysis, our motivation is to suppress the model’s reliance on specific forgery artifacts for detection during fine-tuning, while preserving its ability to identify real images based on the “distributional deviations” in the high-dimensional feature space. To achieve this, we propose masking texture-rich regions, which are areas that generative models typically struggle to synthesize realistically [36] and that often contain model-specific patterns.

For real images, CLIP-ViT learns highly abstract representations rather than relying on specific local textures, so the remaining regions retain sufficient information to effectively cluster real-image features. For AI-generated images, masking model-specific patterns prevents overfitting and encourages the model to rely on the inherent “distributional deviations” between generated and real images across different models. This shifts the fine-tuning objective from capturing the differences between real and generated images in the training set to detecting the deviations from real images in the high-level feature space, thereby exploiting CLIP’s inherent ability to cluster real images and enabling generalized detection across diverse generative models.

Building on this motivation, we propose a simple yet effective **Masking-based Pre-trained model Fine-Tuning strategy (MPFT)** in this work. Specifically, we fine-tune the pre-trained CLIP-ViT with a small amount of data and introduce a Texture-Aware Masking (TAM) mechanism that selectively masks out local regions with rich textures during fine-tuning. As shown in Figure 1 (c) and (d), our method demonstrates strong generalization: the pre-trained CLIP-ViT fine-tuned on only SDV1.4-generated images using our MPFT strategy performs comparably to one fine-tuned directly on images from all involved generative models. Moreover, our method exhibits stable generalization throughout the fine-tuning process (Figure 2, red line). Extensive experiments on both the GenImage [39] and UniversalFakeDetect [23] datasets demonstrate the effectiveness of our approach.

Our main contributions are three-fold as follows:

- **In-depth Analysis of the Frozen Pre-Trained CLIP-ViT.** We perform an analysis and provide the insight that the frozen pre-trained CLIP-ViT achieves strong generalization through effective real image clustering, while also highlighting the necessity and limitations of fine-tuning.
- **A Novel Perspective on AI-generated Image Detection.** Unlike previous methods that rely on low-level artifacts, our method emphasizes “distributional deviations” in high-dimensional feature space, achieving superior generalization across diverse generative models.
- **Effective Fine-tuning strategy.** We propose MPFT, a fine-tuning strategy incorporating a Texture-Aware Masking (TAM) mechanism that masks rich-textured regions, mitigates overfitting, and preserves CLIP-ViT’s intrinsic ability to cluster real images effectively.

## 2. Related Works

### 2.1. Feature Learning-Based Methods

Previous methods based on spatial [7, 13, 19, 32] and frequency [9, 11, 12, 21, 28] domains demonstrated high accuracy in detecting images from the seen generative models but struggled to identify images generated by unseen mod-

els [6, 35]. Recent methods have shifted towards identifying generalizable features that span various generative models. Specifically, LNP [17] discovered that noise patterns in real images exhibit consistent characteristics in the frequency domain, unlike generated images. LGrad [27] transforms images into gradient representations. PatchCraft [36] captures the residual pixel fluctuations between textured and smooth areas. NPR [29] identifies artifacts from the upsampling process. DIRE [33] and LaRE<sup>2</sup> [22] utilize reconstruction errors from diffusion models. In contrast to methods that rely on low-level artifacts, we introduce a novel perspective by focusing on the distributional deviations between real and AI-generated images in high-level, abstract feature representations, thereby achieving superior generalization.

### 2.2. Pre-trained CLIP-based Methods

Another line of research leverages large pre-trained models such as CLIP to enhance generalization in AI-generated image detection. For instance, Ojha [23] proposes using a pre-trained CLIP image encoder with a trainable linear classifier, which helps prevent overfitting and improves generalization. RINE [16] extends this approach by utilizing intermediate-layer features from the frozen CLIP-ViT encoder. FatFormer [18] introduces an adapter to identify local forgery regions and incorporates a contrastive objective between image features and textual prompts. C2P-CLIP [30] injects category-related concepts into the image encoder by integrating the category common prompt. However, these methods generally treat the CLIP image encoder as a feature extractor. In contrast, we conduct a deeper investigation into the intrinsic properties of the pre-trained visual encoder and find that CLIP-ViT naturally clusters real images effectively in a high-level feature space. Based on this observation, our method explicitly exploits this property by fine-tuning the model to identify distributional deviations from real images. This novel perspective, which detects fake images by focusing on their distributional deviations from real images, significantly enhances generalization across diverse generative models.

## 3. Method

In this section, we introduce **Masking-based Pre-trained model Fine-Tuning strategy (MPFT)**, a simple yet effective masking-based pre-trained model fine-tuning strategy. MPFT employs a Texture-Aware Mask (TAM) to mask texture-rich regions—areas where generative models often struggle to generate intricate details, leaving behind model-specific patterns. By masking these regions, MPFT prevents the model from overfitting to such patterns during fine-tuning, encouraging it to focus on the “distributional deviations” between real and generated images. This enhances generalization and effectively leverages the pre-

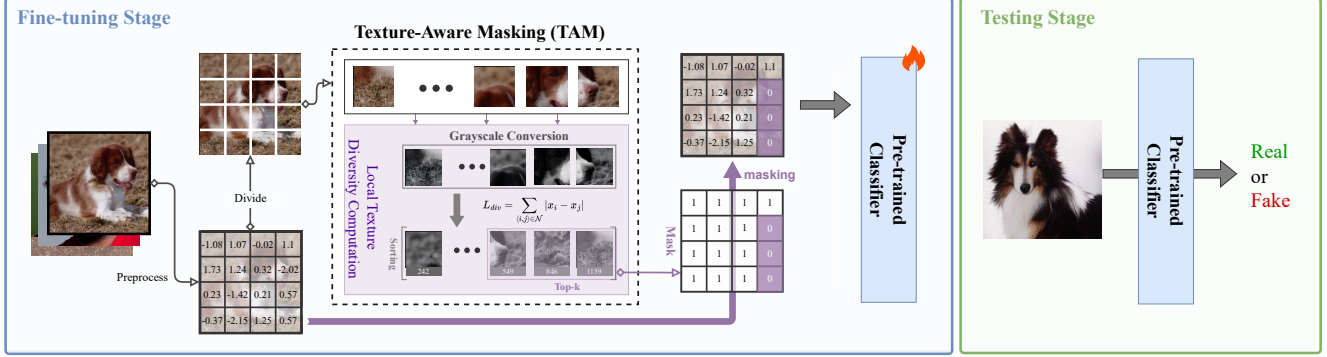


Figure 3. Overview of the Fine-tuning and Testing Pipeline.

trained model's inherent ability to cluster real images.

### 3.1. Texture-Aware Masking (TAM) Mechanism.

Given an RGB image  $X \in \mathbb{R}^{C \times H \times W}$ , we first divide it into  $N$  non-overlapping patches of size  $p \times p$ . For each patch, we convert it to grayscale and compute its local texture diversity  $L_{div}$  [36], defined as the sum of absolute differences between adjacent pixel values along four directions:

$$L_{div} = \sum_{\langle i, j \rangle \in \mathcal{N}} |x_i - x_j| \quad (1)$$

where  $\langle i, j \rangle$  denotes all adjacent pixel pairs within the patch  $x$ , and  $\mathcal{N}$  includes neighbors in the horizontal, vertical, diagonal, and anti-diagonal directions. The full equation is provided in the Appendix B.

Patches are then ranked according to their  $L_{div}$  scores, and the top- $k$  patches with the highest texture complexity are masked by setting the corresponding regions in the binary mask  $M \in \mathbb{R}^{1 \times H \times W}$  to zero, based on the masking ratio  $r_{mask}$ , while the remaining regions are kept as one. The generated mask  $M$  is applied to the input image prior to model fine-tuning. The pseudo-code of the proposed masking mechanism process is provided in Algorithm 1.

### 3.2. Pipeline.

The overview of the pipeline is shown in Figure 3. In the fine-tuning stage, the input image undergoes preprocessing, transforming it into a suitable tensor format for model input. Before feeding the image into the model, the TAM mechanism is applied to all three channels to suppress regions with high texture complexity, as shown in:

$$\begin{aligned} X_{tensor} &= \text{Preprocess}(X) \\ X_{input} &= \text{TAM}(X_{tensor}) \circ X_{tensor} \end{aligned} \quad (2)$$

In this equation,  $X_{tensor}$  represents the preprocessed image tensor,  $\text{TAM}(X_{tensor})$  is the binary mask, and  $X_{input}$  denotes the final input tensor fed into the model. In the testing stage, after preprocessing, the image is directly fed into the fine-tuned model for prediction.

## 4. Experimental Setup

### 4.1. Dataset

To evaluate the effectiveness of our proposed method, we perform an evaluation on the two widely used benchmarks GenImage [39] and UniversalFakeDetect [23].

#### 4.1.1. GenImage.

The GenImage dataset includes images generated by eight different generative models and spans a wide range of image resolutions. In our experiments, we follow the official dataset split by training on images generated by one model

---

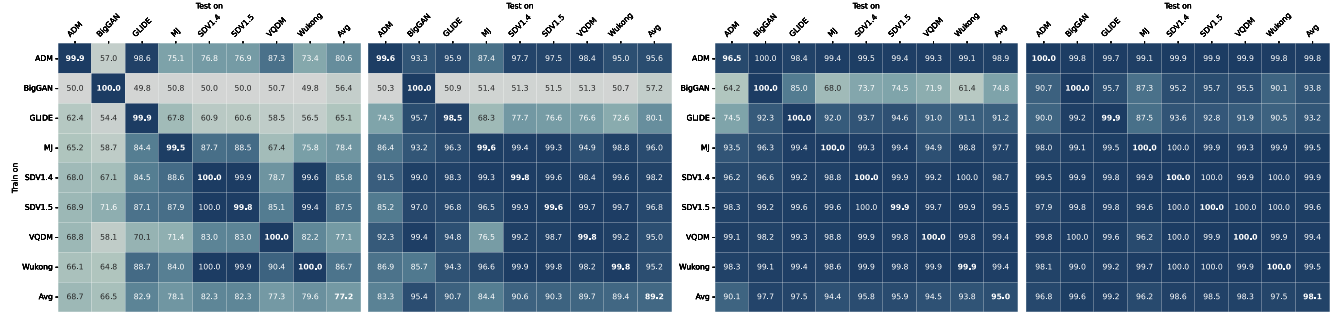
#### Algorithm 1 Texture-Aware Mask Generation

---

**Require:** An RGB image  $x$  of size  $C \times H \times W$ , masking ratio  $r_{mask}$ , patch size  $p$   
**Ensure:** A mask  $M$  of size  $1 \times H \times W$

- 1: Initialize mask  $M \leftarrow \mathbf{1}^{1 \times H \times W}$
- 2: Divide  $x$  into  $N$  non-overlapping patches of size  $C \times p \times p$
- 3: **for**  $k = 1$  to  $N$  **do**
- 4:     Convert the  $k$ -th patch  $x_k$  to grayscale:  $g_k \leftarrow \text{mean}(x_k, \text{channel})$
- 5:     Compute  $L_{div}(k)$  as the sum of absolute differences between adjacent pixels in  $g_k$  (horizontal, vertical, diagonal)
- 6: **end for**
- 7: Sort patch indices in descending order of  $L_{div}$ :  $I \leftarrow \text{argsort}(L_{div}, \text{descending})$
- 8:  $n_{mask} \leftarrow \lfloor N \times r_{mask} \rfloor$
- 9:  $S \leftarrow I[1 : n_{mask}]$  // Indices of selected patches to be masked
- 10: **for** each index  $s$  in  $S$  **do**
- 11:     Compute  $(i, j)$  as the patch's top-left coordinate in  $M$
- 12:     Set  $M[:, i : i + p - 1, j : j + p - 1] \leftarrow 0$
- 13: **end for**
- 14: **return**  $M$

---



(a) Acc Comparison: Left: Direct Fine-Tuned; Right: Fine-Tuned with Our MPFT.

(b) AP Comparison. Left: Fine-tuned Directly; Right: Fine-tuned with our MPFT.

Figure 4. Accuracy (Acc) Across 8 Subsets on GenImage: Comparison of CLIP-ViT with two fine-tuning strategies: direct fine-tuning (base) and fine-tuning with our proposed MPFT method. Models are fine-tuned on a single subset and evaluated on all 8 subsets. The color scale represents performance, with darker shades indicating higher accuracy.

Methods	Ref	Testing Subset								Avg. Acc. (%)
		ADM	BigGAN	GLIDE	MidJourney	SDV1.4	SDV1.5	VQDM	Wukong	
CNN-Spot	CVPR 2020	50.1	46.8	39.8	52.8	96.3	95.9	53.4	78.6	64.2
F3Net	ECCV 2020	49.9	49.9	50.0	50.1	99.9	99.9	49.9	99.9	68.7
Swin-T	ICCV 2021	49.8	57.6	67.6	62.1	99.9	99.8	62.3	99.1	74.8
CLIP-ViT	Base Model*	68.0	67.1	84.5	88.6	100.0	99.9	78.7	99.6	85.8
LaRE <sup>2</sup>	CVPR 2024	61.7	68.7	88.5	74.0	100.0	99.9	97.2	100.0	86.3
UniFD	CVPR 2023	71.9	90.5	85.4	93.9	96.4	96.2	81.6	94.3	88.8
NPR	CVPR 2024	76.9	84.2	89.8	81.0	98.2	97.9	84.1	96.9	88.6
FreqNet	AAAI 2024	66.8	81.4	86.5	89.6	98.8	98.6	75.8	97.3	86.8
FatFormer	CVPR 2024	75.9	55.8	88.0	92.7	100.0	99.9	98.8	99.9	88.9
C2P-CLIP	AAAI 2025	96.4	98.7	99.0	88.2	90.9	97.9	96.5	98.8	<u>95.8</u>
MPFT (CLIP-ViT)	Ours	91.5	99.0	98.3	99.3	99.8	99.6	98.4	99.6	<b>98.2</b>

Table 1. Comparison of Average Accuracy (Avg. Acc) between our method and existing methods on the GenImage test sets. Each model is trained on the SDV1.4 subset and evaluated across all test sets. The results for existing methods are directly cited from [30]. **Bold** and underline represent the best and second-best performance, respectively.

and evaluating generalization performance across all others. Specifically, we sample 800 training images from the original training set for fine-tuning.

#### 4.1.2. UniversalFakeDetect.

The UniversalFakeDetect dataset contains images generated by 19 different generative models, including both GAN-based and diffusion-based models. Following prior work [18, 28], we train only on images generated by ProGAN and adopt a 4-class subset (car, cat, chair, horse) for training, selecting 800 images per class from the original training set.

#### 4.2. Baselines

To comprehensively evaluate our method, we compare it against CLIP-ViT [25] fine-tuned directly (base), as well as various existing forgery detection methods. These include CNN-Spot [32], F3Net [24], Patchfor [2], Swin-T [20], UniFD [23], LGrad [27], NPR [29], LaRE<sup>2</sup>, FreqNet [28], RINE [16], FatFormer [18], and C2P-CLIP [30].

### 4.3. Implementation Details

For training, input images were randomly cropped to 224 × 224, with horizontal flipping and rotation applied for data augmentation. Images that did not meet the minimum crop requirements were expanded by stitching repeated content to achieve the necessary crop size. In contrast, only center cropping was applied during testing. The Adam optimizer [15] with beta parameters (0.9, 0.999) was employed to minimize binary cross-entropy loss. All experiments were conducted on an Nvidia GeForce RTX 3090 GPU. More detailed Implementation details can be found in the Appendix E.

### 4.4. Evaluation metric

In accordance with the protocols outlined in prior methods [22, 23, 30], we use Accuracy (Acc) and Average Precision (AP) as the primary evaluation metrics. To evaluate the model’s generalization capability, we compute the average Acc (Avg. Acc) and average AP (Avg. AP) across datasets

Method	Generative Adversarial Networks							Deep fakes	Low level		Perc. loss		Guided	LDM			Glide			Dalle	Avg. Acc
	Pro GAN	Cycle GAN	Big GAN	Style GAN	Gau GAN	Star GAN	SITD		SAN	CRN	IMLE	200 steps		200 w/cfg	100 steps	100	50	100			
CNN-Spot	100.0	85.2	70.2	85.7	79.0	91.7	53.5	66.7	48.7	86.3	86.3	60.1	54.0	55.0	54.1	60.8	63.8	65.7	55.6	69.6	
Patchfor	75.0	69.0	68.5	79.2	64.2	63.9	75.5	75.1	75.3	72.3	55.3	67.4	76.5	76.1	75.8	74.8	73.3	68.5	67.9	71.2	
F3Net	99.4	76.4	65.3	92.6	58.1	100.0	63.5	54.2	47.3	51.5	51.5	96.2	68.2	75.4	68.8	81.7	83.3	83.1	66.3	71.3	
CLIP-ViT*	100.0	78.1	75.3	85.7	62.6	100.0	55.7	69.0	72.4	49.8	50.3	81.3	87.9	84.6	90.2	70.3	79.0	74.5	89.0	76.6	
LGrad	99.8	85.4	82.9	94.8	72.5	99.6	58.0	62.5	50.0	50.7	50.8	77.5	94.2	95.9	94.8	87.4	90.7	89.6	88.4	80.3	
UniFD	100.0	98.5	94.5	82.0	99.5	97.0	66.6	63.0	57.5	59.5	72.0	70.0	94.2	73.8	94.4	79.1	79.9	78.1	86.8	81.4	
FreqNet	97.9	95.8	90.5	97.5	90.2	93.4	97.4	88.9	59.0	71.9	67.4	86.7	84.6	99.6	65.6	85.7	97.4	88.2	59.1	85.1	
NPR	99.8	95.0	87.6	96.2	86.6	99.8	76.9	66.9	98.6	50.0	50.0	84.6	97.7	98.0	98.2	96.3	97.2	97.4	87.2	87.6	
FatFormer	99.9	99.3	99.5	97.2	99.4	99.8	93.2	81.1	68.0	69.5	69.5	76.0	98.6	94.9	98.7	94.4	94.7	94.2	98.8	90.9	
RINE	100.0	99.3	99.6	88.9	99.8	99.5	80.6	90.6	68.3	89.2	90.6	76.1	98.3	88.2	98.6	88.9	92.6	90.7	95.0	91.3	
C2P-CLIP	100.0	97.3	99.1	96.4	99.2	99.6	93.8	95.6	64.4	93.3	93.3	69.1	99.3	97.3	99.3	95.3	95.3	96.1	98.6	93.8	
MPFT	99.9	99.2	97.3	94.9	97.6	99.7	97.6	94.7	90.9	87.7	84.8	82.0	99.3	97.2	99.5	95.5	96.3	96.8	98.4	<b>94.6</b>	

Table 2. Accuracy (Acc) results of forgery detection methods on UniversalFakeDetect, covering both GANs and diffusion models. **Bold** and underline represent the best and second-best performance, respectively.

Method	Generative Adversarial Networks							Deep fakes	Low level		Perc. loss		Guided	LDM			Glide			Dalle	Avg. AP
	Pro GAN	Cycle GAN	Big GAN	Style GAN	Gau GAN	Star GAN	SITD		SAN	CRN	IMLE	200 steps	200 w/cfg	100 steps	100	50	100				
CNN-Spot	100.0	93.5	84.5	99.5	89.5	98.2	89.0	73.8	59.5	98.2	98.4	73.7	70.6	71.0	70.5	80.7	84.9	82.1	70.6	83.6	
Patchfor	80.9	72.8	71.7	85.8	66.0	69.3	76.6	76.2	76.3	74.5	68.5	75.0	87.1	86.7	86.4	85.4	83.7	78.4	75.6	77.7	
F3Net	100.0	84.3	69.9	99.7	56.7	100.0	78.8	52.9	46.7	63.4	64.4	70.5	73.8	81.7	74.6	89.8	91.0	90.9	71.8	76.9	
LGrad	100.0	94.0	90.7	99.9	79.4	100.0	67.9	59.4	51.4	63.5	69.6	87.1	99.0	99.2	99.2	93.2	95.1	94.9	97.2	86.4	
UniFD	100.0	98.1	94.5	86.7	99.3	99.5	91.7	78.5	67.5	83.1	91.1	79.2	95.8	79.8	95.9	93.9	95.1	94.6	88.5	90.1	
CLIP-ViT*	100.0	95.2	95.9	99.5	95.0	100.0	93.8	85.2	77.4	93.7	97.5	91.2	93.9	90.6	95.3	79.0	85.1	82.1	92.3	91.7	
FreqNet	99.9	99.6	96.1	99.9	99.7	98.6	99.9	94.4	74.6	80.1	75.7	96.3	96.1	100.0	62.3	99.8	99.8	96.4	77.8	92.0	
NPR	100.0	99.5	94.5	99.9	88.8	100.0	84.4	98.0	100.0	50.2	50.2	98.3	99.9	99.9	99.9	99.9	99.9	99.9	99.3	92.8	
FatFormer	100.0	100.0	100.0	99.8	100.0	100.0	98.0	97.9	81.2	99.8	99.9	92.0	99.8	99.1	99.9	99.1	99.4	99.2	99.8	98.2	
RINE	100.0	100.0	99.9	99.4	100.0	100.0	97.9	97.2	94.9	97.3	99.7	96.4	99.8	98.3	99.9	98.8	99.3	98.9	99.3	98.8	
C2P-CLIP	100.0	100.0	100.0	99.5	100.0	100.0	98.6	98.9	84.6	99.9	100.0	94.1	100.0	99.8	100.0	99.7	99.8	99.8	99.9	98.7	
MPFT	100.0	100.0	99.9	99.3	100.0	100.0	96.8	100.0	95.5	100.0	99.9	95.6	99.8	99.4	99.9	98.1	98.8	98.9	99.6	<b>99.0</b>	

Table 3. Average Precision (AP) results of forgery detection methods on UniversalFakeDetect.

from different generative models.

## 5. Results and Analysis

### 5.1. Evaluation of Performance over Base method

To evaluate the effectiveness of our proposed method, we conducted comparative experiments on the GenImage dataset, comparing the base CLIP-ViT (fine-tuned directly) with the version fine-tuned using our method. The models were fine-tuned on one subset and evaluated across all eight subsets. Additionally, we evaluated the models fine-tuned on images generated by all eight generative models to assess their generalization capability further. As shown in Figure 4, our method demonstrates exceptional gener-

alization performance, achieving a 12.0% improvement in average Acc and a 3.1% improvement in average AP compared to the directly fine-tuned version. Among all subsets, the model fine-tuned on SDV1.4 achieves the best overall performance, while fine-tuning on BigGAN leads to limited generalization due to its low resolution (128x128) and clear separability from real images, in line with prior reports [22, 39].

### 5.2. Comparison with Existing Methods

To further demonstrate the effectiveness of our proposed method, we compared its performance with recent methods on both GenImage and UniversalFakeDetect datasets, following the previous method [30].

Masking Strategy	GenImage		UniversalFakeDetect	
	Avg.Acc	Avg.AP	Avg.Acc	Avg.AP
CutOut	90.3	99.4	91.3	98.0
GridMask	92.8	99.6	91.3	97.2
Random Masking	91.1	99.6	93.1	98.1
TAM (Low)	87.8	97.8	90.6	98.2
TAM (Both)	93.2	99.6	92.5	98.4
<b>TAM (Ours)</b>	<b>98.2</b>	<b>99.9</b>	<b>94.6</b>	<b>99.0</b>

Table 4. Average accuracy and average AP evaluated on the GenImage and UniversalFakeDetect datasets under different masking strategies. Top-performing results are highlighted in bold. TAM (Low) masks regions with the least texture, whereas TAM (Both) masks both high- and low-texture regions equally, with the same total masking ratio.

### 5.2.1. Evaluation on GenImage.

We follow existing methods [30, 39] and use the SDV1.4 for fine-tuning. The results of accuracy (Acc) are shown in Table 6. Notably, our method achieves 98.2% Avg. Acc using only 1% of the training data, outperforming all existing methods and reaching a 2.4% improvement in Avg.Acc compared to the current SOTA method, C2P-CLIP [30]. This demonstrates that our method achieves exceptional generalization by enabling the pre-trained CLIP-ViT to focus on the “distributional deviations” between real and AI-generated images in the high-dimensional feature space.

### 5.2.2. Evaluation on UniversalFakeDetect.

Table 2 and Table 3 present the accuracy (Acc) and average precision (AP) results. Our method outperforms all existing methods, achieving an Avg. Acc of 94.6% and an Avg. AP of 99.0%. Specifically, CLIP-ViT fine-tuned using our MPFT surpasses the directly fine-tuned version by 18.0% in Avg. Acc and 7.3% in Avg. AP. Moreover, our approach outperforms the latest SOTA method in both Avg. Acc and Avg. AP. These results further demonstrate the effectiveness of our approach.

## 5.3. Ablation Study

In this section, we present comprehensive ablation studies on both the GenImage [39] and UniversalFakeDetect [23] datasets to analyze the impact of different fine-tuning data volumes and masking strategies. Additional experiments are in the Appendix C.

### 5.3.1. Impact of Different Masking Strategies.

To further evaluate our proposed fine-tuning framework, we investigate the effects of different masking strategies, as shown in Table 4. We compare several widely used masking methods—CutOut [8], GridMask [3], and Random Erasing [37]—with our proposed Texture-Aware Masking

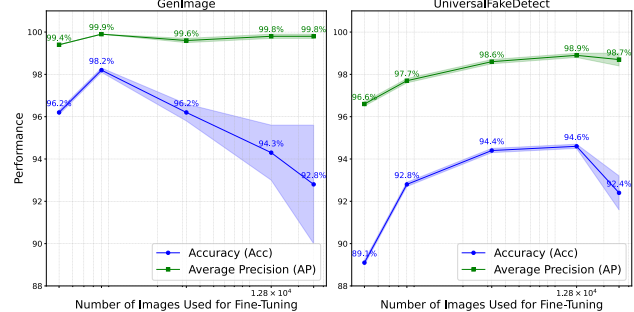


Figure 5. Average Acc and average AP of CLIP-ViT fine-tuned with our method using different numbers of images (400, 800, 3200, 12800, and 25600)—with an equal split between real and generated images—evaluated on the GenImage and UniversalFakeDetect. To reflect the stability of the model’s generalization, we report the results averaged over the last five epochs.

(TAM) under various masking configurations. The experimental results demonstrate that our fine-tuning strategy, MPFT, is compatible with all masking methods, each achieving satisfactory performance. However, our TAM consistently outperforms them. This suggests that while masking arbitrary regions of an image can constrain the model from overfitting generative model-specific patterns, explicitly masking texture-rich areas is more effective. Furthermore, the results of masking low-texture regions or jointly masking both high- and low-texture regions further confirm that models tend to rely on texture-rich areas to distinguish real images from AI-generated ones.

### 5.3.2. Impact of Fine-tuning Data Volume.

To investigate the impact of fine-tuning data volume, we analyze the performance of CLIP-ViT fine-tuned with varying data amounts using our method, as shown in Figure 5. The results show that the pre-trained CLIP-ViT achieves optimal generalization with a small amount of fine-tuning data (800 samples for GenImage and 3200 or 12800 for UniversalFakeDetect). As the data volume increases, generalization performance becomes unstable and deteriorates. This is due to the model’s tendency to overfit local forgery artifacts when exposed to more data during fine-tuning, shifting the decision criterion from “real image distribution” to “specific artifacts,” which leads to overfitting and reduced generalization.

## 5.4. Robustness Analysis

To evaluate the robustness of our method under various perturbations, we applied noise, blurring, JPEG compression, and random cropping, with more details provided in Appendix D. The results, presented in Table 5, show that noise and blurring significantly degrade model performance, with noise having the most pronounced effect. In contrast, random cropping and JPEG compression have minimal impact

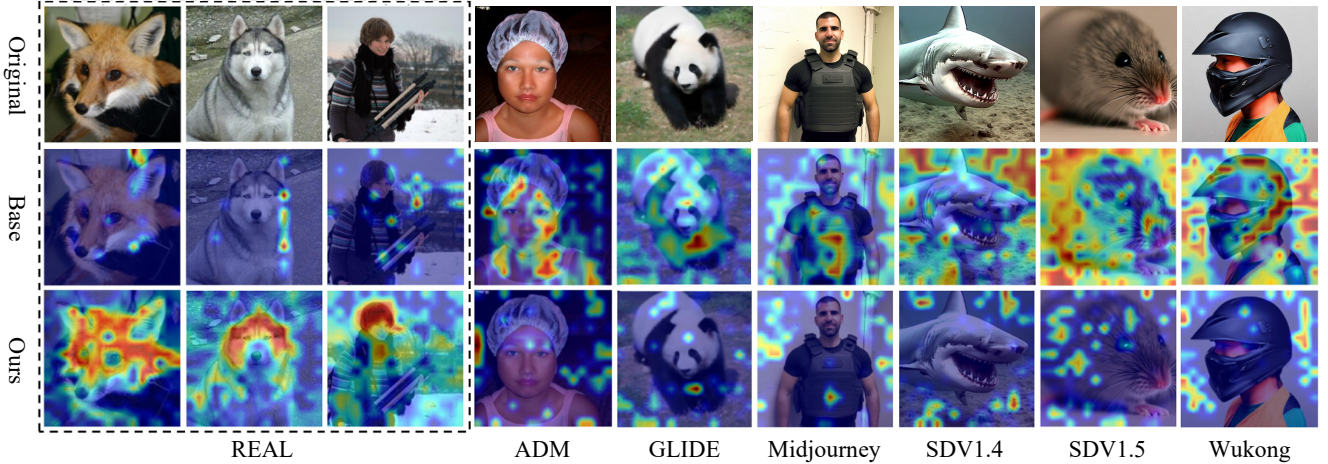


Figure 6. Class Activation Map (CAM) [38] visualization for real and AI-generated images, comparing CLIP-ViT fine-tuned directly (base) with SDV1.4 and fine-tuned using our proposed MPFT.

				w/Blur	w/Cropping	w/JPEG	w/Noise	Avg.Acc. (%)	Avg.AP. (%)
				GenImage					
✓	✗	✗	✗	81.1 (17.1↓)	87.7 (12.2↓)				
✗	✓	✗	✗	97.0 (1.2↓)	99.5 (0.4↓)				
✗	✗	✓	✗	89.2 (9.0↓)	3.2 (1.09↓)				
✗	✗	✗	✓	79.1 (19.1↓)	90.5 (9.4↓)				
✓	✓	✓	✓	84.9 (13.3↓)	89.3 (10.6↓)				
UniversalFakeDetect									
✓	✗	✗	✗	84.5 (10.1↓)	90.5 (8.5↓)				
✗	✓	✗	✗	92.1 (2.5↓)	98.4 (0.6↓)				
✗	✗	✓	✗	90.2 (4.4↓)	95.9 (3.1↓)				
✗	✗	✗	✓	81.3 (13.3↓)	91.4 (7.5↓)				
✓	✓	✓	✓	87.2 (7.4↓)	94.3 (4.7↓)				

Table 5. Average Accuracy (Avg.Acc) and Average Precision (Avg.Ap) evaluated on UniversalFakeDetect under various perturbations.

on performance, indicating that our method is more sensitive to image quality and exhibits strong robustness to geometric transformations. Additionally, to simulate real-world conditions, we sequentially applied all four perturbations—noise, blurring, JPEG compression, and random cropping—on both the training and test sets. Although our method’s performance degrades in this real-world scenario, it still maintains relatively high accuracy.

### 5.5. Class Activation Map Visualization

We conducted class activation map (CAM) analysis on both real and generated images to further investigate our method, as shown in Figure 6. The CLIP-ViT model fine-tuned directly on SDV1.4 responds more strongly to generated images, showing less attention to real images. This sug-

gests that the directly fine-tuned model overfits to generative model-specific patterns within the generated images, focusing primarily on local artifacts, which diminishes its ability to generalize across different generative models. In contrast, when fine-tuning CLIP-ViT using our method, the model exhibits strong attention to real images and minimal response to AI-generated images. The visualization results further confirm that our method effectively guides the pre-trained CLIP-ViT to detect AI-generated images by referencing real images and recognizing deviations from their distributions in the highly abstract feature space, rather than relying on local forgery details.

## 6. Conclusion

In this paper, we propose a simple yet effective Masking-based Pre-trained model Fine-Tuning (MPFT) strategy that enhances the generalization of AI-generated image detection. By introducing a Texture-Aware Masking (TAM) mechanism, we leverage the inherent strengths of the pre-trained CLIP-ViT to focus on the “distributional deviations” between real and generated images in a high-level feature space. Our method shifts the task from distinguishing real and generated images to identifying real images, which enables better generalization across a wide range of generative models. Extensive experiments on the GenImage and UniversalFakeDetect datasets demonstrate that our method outperforms existing approaches, showcasing exceptional generalization ability.

**Limitations.** Admittedly, our method is sensitive to the quality of the generated images used for training. If the training data contains lower-quality images, it can negatively impact its performance. In future work, we aim to develop more robust methods that can maintain strong performance even with lower-quality training images.

## References

[1] Midjourney. <https://www.midjourney.com/home/>, 2022. 1

[2] Lucy Chai, David Bau, Ser-Nam Lim, and Phillip Isola. What makes fake images detectable? understanding properties that generalize. In *Computer vision–ECCV 2020: 16th European conference, Glasgow, UK, August 23–28, 2020, proceedings, part XXVI 16*, pages 103–120. Springer, 2020. 5

[3] Pengguang Chen, Shu Liu, Hengshuang Zhao, Xingquan Wang, and Jiaya Jia. Gridmask data augmentation. *arXiv preprint arXiv:2001.04086*, 2020. 7

[4] Yingjian Chen, Lei Zhang, and Yakun Niu. Forgelens: Data-efficient forgery focus for generalizable forgery image detection. In *Proceedings of the IEEE/CVF International Conference on Computer Vision (ICCV)*, pages 16270–16280, 2025. 2

[5] Riccardo Corvi, Davide Cozzolino, Giovanni Poggi, Koki Nagano, and Luisa Verdoliva. Intriguing properties of synthetic images: from generative adversarial networks to diffusion models. In *Proceedings of the IEEE/CVF Conference on Computer Vision and Pattern Recognition*, pages 973–982, 2023. 2

[6] Davide Cozzolino, Justus Thies, Andreas Rössler, Christian Riess, Matthias Nießner, and Luisa Verdoliva. Forensictransfer: Weakly-supervised domain adaptation for forgery detection. *arXiv preprint arXiv:1812.02510*, 2018. 3

[7] Xin Deng, Bihe Zhao, Zhenyu Guan, and Mai Xu. New finding and unified framework for fake image detection. *IEEE Signal Processing Letters*, 30:90–94, 2023. 1, 3

[8] Terrance DeVries and Graham W Taylor. Improved regularization of convolutional neural networks with cutout. *arXiv preprint arXiv:1708.04552*, 2017. 7

[9] Joel Frank, Thorsten Eisenhofer, Lea Schönherr, Asja Fischer, Dorothea Kolossa, and Thorsten Holz. Leveraging frequency analysis for deep fake image recognition. In *International conference on machine learning*, pages 3247–3258. PMLR, 2020. 3, 12

[10] Jonathan Ho, Ajay Jain, and Pieter Abbeel. Denoising diffusion probabilistic models. *Advances in neural information processing systems*, 33:6840–6851, 2020. 1

[11] Yonghyun Jeong, Doyeon Kim, Seungjai Min, Seongho Joe, Youngjune Gwon, and Jongwon Choi. Bihpf: Bilateral high-pass filters for robust deepfake detection. In *Proceedings of the IEEE/CVF Winter Conference on Applications of Computer Vision*, pages 48–57, 2022. 1, 3

[12] Yonghyun Jeong, Doyeon Kim, Youngmin Ro, and Jongwon Choi. Freqgan: robust deepfake detection using frequency-level perturbations. In *Proceedings of the AAAI conference on artificial intelligence*, pages 1060–1068, 2022. 3

[13] Yan Ju, Shan Jia, Jialing Cai, Haiying Guan, and Siwei Lyu. Glff: Global and local feature fusion for ai-synthesized image detection. *IEEE Transactions on Multimedia*, 2023. 1, 3

[14] Sohail Ahmed Khan and Duc-Tien Dang-Nguyen. Clipping the deception: Adapting vision-language models for universal deepfake detection. In *Proceedings of the 2024 International Conference on Multimedia Retrieval*, pages 1006–1015, 2024. 1

[15] Diederik P Kingma. Adam: A method for stochastic optimization. *arXiv preprint arXiv:1412.6980*, 2014. 5

[16] Christos Koutlis and Symeon Papadopoulos. Leveraging representations from intermediate encoder-blocks for synthetic image detection. *arXiv preprint arXiv:2402.19091*, 2024. 1, 3, 5

[17] Bo Liu, Fan Yang, Xiuli Bi, Bin Xiao, Weisheng Li, and Xinbo Gao. Detecting generated images by real images. In *European Conference on Computer Vision*, pages 95–110. Springer, 2022. 3

[18] Huan Liu, Zichang Tan, Chuangchuang Tan, Yunchao Wei, Jingdong Wang, and Yao Zhao. Forgery-aware adaptive transformer for generalizable synthetic image detection. In *Proceedings of the IEEE/CVF Conference on Computer Vision and Pattern Recognition*, pages 10770–10780, 2024. 1, 2, 3, 5, 11

[19] Zhengze Liu, Xiaojuan Qi, and Philip HS Torr. Global texture enhancement for fake face detection in the wild. In *Proceedings of the IEEE/CVF conference on computer vision and pattern recognition*, pages 8060–8069, 2020. 3

[20] Ze Liu, Yutong Lin, Yue Cao, Han Hu, Yixuan Wei, Zheng Zhang, Stephen Lin, and Baining Guo. Swin transformer: Hierarchical vision transformer using shifted windows. In *Proceedings of the IEEE/CVF international conference on computer vision*, pages 10012–10022, 2021. 5

[21] Yuchen Luo, Yong Zhang, Junchi Yan, and Wei Liu. Generalizing face forgery detection with high-frequency features. In *Proceedings of the IEEE/CVF conference on computer vision and pattern recognition*, pages 16317–16326, 2021. 1, 3

[22] Yunpeng Luo, Junlong Du, Ke Yan, and Shouhong Ding. Lare<sup>2</sup>: Latent reconstruction error based method for diffusion-generated image detection. In *Proceedings of the IEEE/CVF Conference on Computer Vision and Pattern Recognition*, pages 17006–17015, 2024. 3, 5, 6

[23] Utkarsh Ojha, Yuheng Li, and Yong Jae Lee. Towards universal fake image detectors that generalize across generative models. In *Proceedings of the IEEE/CVF Conference on Computer Vision and Pattern Recognition*, pages 24480–24489, 2023. 1, 2, 3, 4, 5, 7, 11

[24] Yuyang Qian, Guojun Yin, Lu Sheng, Zixuan Chen, and Jing Shao. Thinking in frequency: Face forgery detection by mining frequency-aware clues. In *European conference on computer vision*, pages 86–103. Springer, 2020. 5

[25] Alec Radford, Jong Wook Kim, Chris Hallacy, Aditya Ramesh, Gabriel Goh, Sandhini Agarwal, Girish Sastry, Amanda Askell, Pamela Mishkin, Jack Clark, et al. Learning transferable visual models from natural language supervision. In *International conference on machine learning*, pages 8748–8763. PMLR, 2021. 1, 2, 5

[26] Robin Rombach, Andreas Blattmann, Dominik Lorenz, Patrick Esser, and Björn Ommer. High-resolution image

synthesis with latent diffusion models. In *Proceedings of the IEEE/CVF conference on computer vision and pattern recognition*, pages 10684–10695, 2022. 1

[27] Chuangchuang Tan, Yao Zhao, Shikui Wei, Guanghua Gu, and Yunchao Wei. Learning on gradients: Generalized artifacts representation for gan-generated images detection. In *Proceedings of the IEEE/CVF Conference on Computer Vision and Pattern Recognition*, pages 12105–12114, 2023. 3, 5, 11

[28] Chuangchuang Tan, Yao Zhao, Shikui Wei, Guanghua Gu, Ping Liu, and Yunchao Wei. Frequency-aware deepfake detection: Improving generalizability through frequency space domain learning. In *Proceedings of the AAAI Conference on Artificial Intelligence*, pages 5052–5060, 2024. 2, 3, 5

[29] Chuangchuang Tan, Yao Zhao, Shikui Wei, Guanghua Gu, Ping Liu, and Yunchao Wei. Rethinking the up-sampling operations in cnn-based generative network for generalizable deepfake detection. In *Proceedings of the IEEE/CVF Conference on Computer Vision and Pattern Recognition*, pages 28130–28139, 2024. 3, 5

[30] Chuangchuang Tan, Renshuai Tao, Huan Liu, Guanghua Gu, Baoyuan Wu, Yao Zhao, and Yunchao Wei. C2p-clip: Injecting category common prompt in clip to enhance generalization in deepfake detection. In *Proceedings of the AAAI Conference on Artificial Intelligence*, pages 7184–7192, 2025. 1, 3, 5, 6, 7, 11

[31] Laurens Van der Maaten and Geoffrey Hinton. Visualizing data using t-sne. *Journal of machine learning research*, 9(11), 2008. 1

[32] Sheng-Yu Wang, Oliver Wang, Richard Zhang, Andrew Owens, and Alexei A Efros. Cnn-generated images are surprisingly easy to spot... for now. In *Proceedings of the IEEE/CVF conference on computer vision and pattern recognition*, pages 8695–8704, 2020. 3, 5

[33] Zhendong Wang, Jianmin Bao, Wengang Zhou, Weilun Wang, Hezhen Hu, Hong Chen, and Houqiang Li. Dire for diffusion-generated image detection. In *Proceedings of the IEEE/CVF International Conference on Computer Vision*, pages 22445–22455, 2023. 3

[34] Shilin Yan, Ouxiang Li, Jiayin Cai, Yanbin Hao, Xiaolong Jiang, Yao Hu, and Weidi Xie. A sanity check for ai-generated image detection. *arXiv preprint arXiv:2406.19435*, 2024. 2

[35] Xu Zhang, Svebor Karaman, and Shih-Fu Chang. Detecting and simulating artifacts in gan fake images. In *2019 IEEE international workshop on information forensics and security (WIFS)*, pages 1–6. IEEE, 2019. 3

[36] Nan Zhong, Yiran Xu, Sheng Li, Zhenxing Qian, and Xinpeng Zhang. Patchcraft: Exploring texture patch for efficient ai-generated image detection. *arXiv preprint arXiv:2311.12397*, 2023. 2, 3, 4

[37] Zhun Zhong, Liang Zheng, Guoliang Kang, Shaozi Li, and Yi Yang. Random erasing data augmentation. In *Proceedings of the AAAI conference on artificial intelligence*, pages 13001–13008, 2020. 7

[38] Bolei Zhou, Aditya Khosla, Agata Lapedriza, Aude Oliva, and Antonio Torralba. Learning deep features for discriminative localization. In *Proceedings of the IEEE conference on computer vision and pattern recognition*, pages 2921–2929, 2016. 8

[39] Mingjian Zhu, Hanting Chen, Qiangyu Yan, Xudong Huang, Guanyu Lin, Wei Li, Zhijun Tu, Hailin Hu, Jie Hu, and Yunhe Wang. Genimage: A million-scale benchmark for detecting ai-generated image. *Advances in Neural Information Processing Systems*, 36, 2024. 2, 3, 4, 6, 7, 11, 12

## Appendix

### A. Dataset Details

#### A.1. GenImage

GenImage [39] consists of subsets generated by 8 different generative models, which are split into training and testing sets. In this work, we have used only a small portion of the training data for fine-tuning. Detailed data can be found in Table 6.

Generative Models	Train Count	Test Count	Neg%
ADM	800	3,200	50%
BigGAN	800	3,200	50%
GLIDE	800	3,200	50%
MidJourney	800	3,200	50%
Stable Diffusion V1.4	800	3,200	50%
Stable Diffusion V1.5	800	3,200	50%
VQDM	800	3,200	50%
Wukong	800	3,200	50%

Table 6. Statistics of the GenImage Dataset. We report the training size and testing size of each subset, and the proportion of negative samples.

#### A.2. UniversalFakeDetect

UniversalFakeDetect [23] includes image subsets generated by 19 different generative models, covering both GAN-based and diffusion-based methods. For our experiments, we use ProGAN as the training set and adopt a 4-class subset (car, cat, chair, horse) as in previous works [18, 27, 30]. During fine-tuning, we randomly select a small portion of data from each class. Details of the dataset are provided in Table 7.

### B. Full Equation for the Calculation of $L_{div}$

$$\begin{aligned}
 L_{div} = & \sum_{i=1}^M \sum_{j=1}^{M-1} |x_{i,j} - x_{i,j+1}| \\
 & + \sum_{i=1}^{M-1} \sum_{j=1}^M |x_{i,j} - x_{i+1,j}| \\
 & + \sum_{i=1}^{M-1} \sum_{j=1}^{M-1} |x_{i,j} - x_{i+1,j+1}| \\
 & + \sum_{i=1}^{M-1} \sum_{j=1}^{M-1} |x_{i+1,j} - x_{i,j+1}|.
 \end{aligned}$$

### C. Additional Experiments

In this section, we present additional experiments, including the impact of masking parameters and the influence of

Generative Models	Size	Class Count	Neg%
<b>Training Set</b>			
ProGAN	3,200 for each	car, cat, chair, horse	50%
<b>Testing Set</b>			
ProGAN	8,000	20	50%
CycleGAN	2,642	6	50%
BigGAN	4,000	N/A	50%
StyleGAN	11,982	3	50%
GauGAN	10,000	N/A	50%
StarGAN	3,998	N/A	50%
Deepfakes	5,405	N/A	49.9%
SITD	360	N/A	50%
SAN	438	N/A	50%
CRN	12,764	N/A	50%
IMLE	12,764	N/A	50%
Guided	2,000	N/A	50%
LDM 200 steps	3,000	N/A	33.3%
LDM 200 w/CFG	3,000	N/A	33.3%
LDM 100 steps	3,000	N/A	33.3%
Glide-100-27	3,000	N/A	33.3%
Glide-50-27	3,000	N/A	33.3%
Glide-100-10	3,000	N/A	33.3%
DALL-E	3,000	N/A	33.3%

Table 7. Statistics of the UniversalFakeDetect Dataset. We report the size of each subset, the number of classes, and the proportion of negative samples.

different training classes in ProGAN on generalization performance.

#### C.1. Effect of Masking Ratio $r_{mask}$ and Patch Size $p$

We conducted ablation experiments to evaluate the effects of different masking ratios  $r_{mask}$ . To increase data variability during training, the masking ratio was randomly selected within a specified range. The results are presented in Table 8. On GenImage, a masking ratio covering 60%-80% of the image area yielded the best performance. For UniversalFakeDetect, a lower masking ratio achieved the best results. This is due to the relatively low image quality in the ProGAN training set of UniversalFakeDetect, as well as the smaller image size. Excessive masking impairs feature extraction, leading to performance degradation.

Additionally, for the masking patch size  $p$ , we initially set it to 14, matching the patch size used in the CLIP-ViT pre-training. However, we also conducted additional ablation studies to comprehensively investigate the influence of different patch sizes at the optimal masking ratio setting on GenImage and UniversalFakeDetect, as shown in Figure 7. The results demonstrate that a patch size of 14 achieves the best performance, as expected, while both larger and smaller patch sizes lead to performance degradation.

Masking Ratio $r_{mask}$	GenImage		UniversalFakeDetect	
	Avg.Acc	Avg.AP	Avg.Acc	Avg.AP
(0.0, 0.2)	91.6	99.7	91.7	98.3
(0.0, 0.4)	96.2	99.7	94.6	99.0
(0.0, 0.6)	93.6	99.6	94.5	98.9
(0.0, 0.8)	93.9	99.8	91.1	98.0
(0.0, 1.0)	89.6	99.7	92.2	98.6
(0.2, 0.4)	93.7	99.7	91.5	98.4
(0.4, 0.6)	95.8	99.8	93.0	97.3
(0.6, 0.8)	98.2	99.9	69.4	82.4
(0.8, 1.0)	90.7	99.7	65.2	87.8

Table 8. Avg. Acc and Avg. AP on GenImage and UniversalFakeDetect, with variations in masking ratio.

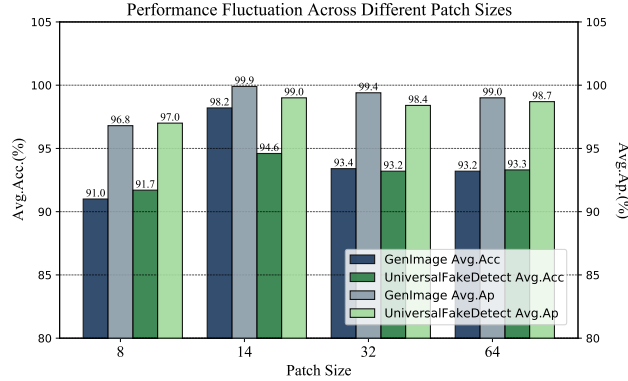


Figure 7. Avg. Acc and Avg. AP on GenImage and UniversalFakeDetect, with variations in masking patch size.

## D. Robustness Analysis

In this section, we present robustness experiments to evaluate the effects of various perturbations on model performance, following the methodology outlined by Frank *et al.* [9]. These experiments are conducted on the GenImage [39] and UniversalFakeDetect.

### D.1. Perturbations

**Noise:** Random Gaussian noise is added to the input images by selecting a variance value from a uniform distribution within the range [5.0, 20.0], controlling the noise intensity. This results in a noisy image with the same dimensions as the original, but with random variations in pixel intensity.

**Blurring:** Gaussian blur is applied to the input images using a randomly selected kernel size from the set 3, 5, 7, 9. Larger kernel sizes produce stronger blurring effects.

**Compression:** JPEG compression is applied to the input images by first selecting a random quality factor between 10 and 75. The image is then encoded into JPEG format with this quality factor, introducing lossy compression.

**Cropping:** A random crop is applied to the input images

by selecting a percentage between 5% and 20%, determining the crop size in both the x and y directions. The image is then resized to its original dimensions using cubic interpolation.

## E. Implementation Hyperparameter Details

To ensure the reproducibility of our experimental results, we provide a complete list of all hyperparameters used during training, as shown in Table 9.

Hyperparameter	Universal FakeDetect	GenImage
seed	3407	3407
batch_size	4	4
epochs	10	10
learning_rate	$1 \times 10^{-6}$	$1 \times 10^{-5}$
lr_decay_step	1	1
lr_decay_factor	0.5	0.5
masking_ratio	(0.0, 0.4)	(0.6, 0.8)
patch_size	14	14

Table 9. Hyperparameters.